Pronounced momentum shift against the radiation pressure in strong-field sequential double ionization

Jingkun Xu,[1,*] Jintai Liang,[1,*] Xiaomeng Ma,[2,*] Kunlong Liu,[1,†] Yingbin Li,[3,‡] Chuanpeng Cao,[1] Min Li ⬤,[1] Benhai Yu,[3]
Yueming Zhou ⬤,[1,§] and Peixiang Lu[1,4]

[1]*School of Physics and Wuhan National Laboratory for Optoelectronics, Huazhong University of Science and Technology,
Wuhan 430074, China*
[2]*Department of Physics and Mechanical and Electrical Engineering, Hubei University of Education, Wuhan 430205, China*
[3]*College of Physics and Electronic Engineering, Xinyang Normal University, Xinyang 464000, China*
[4]*Optics Valley Laboratory, Hubei 430074, China*

The nondipole effect in strong-field sequential double ionization of an Ar atom is investigated with the Heisenberg-core potential classical ensemble model, in which the magnetic component of the laser field is included. We show that the magnetic field induces a nonzero displacement of the electron along the laser propagation direction when the electron is driven back by the linearly polarized laser field. This displacement significantly affects the electron-ion rescattering, manifesting as a pronounced linear momentum transfer against the radiation pressure for the low-energy photoelectron. Such phenomenon depends on the laser intensity and traveling time of the photoelectrons. Particularly, a larger negative linear momentum transfer for low-energy electrons is obtained in a more intense laser field with longer pulse duration, in which case it would be beneficial to observe the nondipole effect in experiment.

I. INTRODUCTION

Strong-field ionization is one of the most fundamental processes in laser-matter interactions and has served as a powerful tool to study the structure and dynamics of matter. For a theoretical description of strong-field ionization, the electric dipole approximation is commonly adopted to facilitate calculations. In this approximation, the laser field is described by a spatially homogeneous vector potential $\mathbf{A}(t)$. Thus, the magnetic field effect is neglected as $\mathbf{B}(t) = \nabla \times \mathbf{A}(t) = 0$. However, as the magnetic field component of the Lorentz force acting on the electron exposed to the laser field depends on its drift velocity, the magnetic field effect is non-negligible in the intense laser field wherein the electron's velocity is large [1,2]. Therefore, the dipole approximation breaks down in the high-intensity long-wavelength limit because of the onset of the magnetic field effect.

Already in 1998, the nondipole effect in strong-field ionization was investigated [3]. Recent experimental [4–12] and theoretical [13–17] works have made great progress in revealing the role of the magnetic field in strong-field ionization. For example, it has been demonstrated that the magnetic field could induce an observable energy shift of the bound state and continuum state in atoms. This energy shift manifests as the shift of the interference fringes in the photoelectron momentum distribution (PEMD) [18–22]. Moreover, the magnetic field effect also induces an asymmetric PEMD along the laser propagation direction (z axis in our work). This asymmetric PEMD shows up as a nonzero expectation value $\langle p_z \rangle$ along the z axis. This expectation value $\langle p_z \rangle$ represents the linear momentum transfer from the photon to the photoelectrons. For recollision-free ionization, the linear momentum transfer law is formulated as $\langle p_z \rangle \approx E_e/c + I_p/(3c)$ [9,15], where E_e is the electron's kinetic energy and I_p is the ionization potential. The term E_e/c results from the classical Lorentz force induced by the magnetic field acting on the ionized electron [4,13], and the additional term $I_p/(3c)$ originates from the action of the magnetic field on the electron during the tunneling process [8,9,14–17]. In the case of strong-field ionization by a linearly polarized laser pulse, the electron could be driven back and rescatter with the core [23,24]. This rescattering significantly changes the result of the the magnetic field effect, wherein a backward-shifted narrow cusp in the PEMD along the laser propagation direction was observed [5,12,25–29]. In this circumstance, the momentum transfer $\langle p_z \rangle$ strongly depends on the details of the rescattering process. For the photoelectrons with energies lower than $2U_p$ (U_p is the ponderomotive potential of the laser field), the term $I_p/(3c)$ vanishes, $\langle p_z \rangle \approx E_e/c$ [9,11,30]. For the electrons with energies larger than $2U_p$, the photon momentum transfer $\langle p_z \rangle$ remains constant as a function of E_e for the He atom [31], but shows a V-shape structure for the Xe atom [11].

Recently, the magnetic field effect in strong-field double ionization has also attracted much attention. It has been shown that the recollision is a sensitive probe of the magnetic field effects in nonsequential double ionization (NSDI), and the results of the magnetic field in NSDI reveal the details of

---

*These authors contributed equally to this work.
†liukunlong@hust.edu.cn
‡liyingbin2008@163.com
§zhouymhust@hust.edu.cn

the recollision process [10,32–36]. In this paper, we studied the magnetic field effect in strong-field sequential double ionization (SDI). In the high laser intensity region where the second electron of the atom can be ionized through tunneling, SDI dominates, even in the linearly polarized laser field. In this case, the hard recollision in NSDI is avoided. Instead, the soft rescattering of both electrons with the parent ion after tunneling ionization is prevalent. We studied the effect of the magnetic effect on the soft rescattering in SDI. By incorporating the magnetic field effect into our previous Heisenberg-core potential classical ensemble model, we surveyed the signatures of the magnetic field on the longitudinal (along the laser propagation direction) momentum of the two electrons. Our results show that the magnetic field induces a pronounced momentum shift against the laser propagation direction for low-energy electrons in the linearly polarized laser pulse. More interestingly, this shift increases as the laser intensity increases. By tracing the trajectories of the photoelectrons, we show that the shift is ascribed to the displacement of the electrons along the laser propagation direction, induced by the magnetic field. There was a positive displacement along the laser propagation direction when the electrons returned back to the the parent ion, and the Coulomb interaction during the soft rescattering imposed a negative longitudinal momentum to the electrons. This displacement increases with the laser intensity and the pulse duration, and, as a result, there is a larger negative linear momentum transfer in the more intense laser pulse with longer duration.

II. METHODS

We study strong-field SDI using the Heisenberg-core potential classical ensemble model (HPCM) [37–43]. In the classical description of a two-electron atom, one electron often drops deeply into the nuclear potential well, leading to the autoionization of the other electron. The Heisenberg-core potential was introduced to avoid the autoionization of the two- and multielectron systems. It introduced the Heisenberg's uncertainty principle in a quantum mechanism into the classical atoms with a potential, which is referred as the Heisenberg-core potential. With this potential, the classical two-electron atom is stable. Moreover, the ionization potentials of the two electrons can be matched with the real atoms by adjusting the parameters in the Heisenberg-core potential. This model has been successful in revealing the electron dynamics in strong-field double and multiple ionization. Here, we include the magnetic field in describing the laser-atom interaction to account for the nondipole effect. In this paper, we choose argon as the target atom. However, the dynamics and the conclusions are similar to other atoms. In this model, the field-free Hamiltonian of the two-bound-electron system is written as (atomic units are used, unless otherwise stated)

$$H_1 = \sum_{i=1,2} \left[\frac{\mathbf{p}_i^2}{2} + V_{ne} + V_H(r_i, p_i) \right] + V_{ee}, \quad (1)$$

where $V_{ne} = -2/r_i$ is the ion core-electron potential energy and $V_{ee} = 1/|\mathbf{r}_1 - \mathbf{r}_2|$ is the electron-electron potential energy. $\mathbf{r}_i$ and $\mathbf{p}_i$, respectively, represent the position and the canonical momentum of the ith electron. $V_H(r_i, p_i)$ is the

Heisenberg core potential, which is expressed as

$$V_H(r_i, p_i) = \frac{\xi^2}{4\alpha r_i^2} \exp \left\{ \alpha \left[1 - \left(\frac{r_i p_i}{\xi} \right)^4 \right] \right\}. \quad (2)$$

Here, the parameter α indicates the rigidity of the Heisenberg core, and ξ is chosen to make the minimum of the Hamiltonian H_1 equal to the ground-state energy of the atom. In our calculations, we set $\alpha = 2$ and $\xi = 1.225$ [38], corresponding to the Ar atom, i.e., the sum of the first and the second ionization potentials $(I_{p1} + I_{p2})$ equals -1.59 a.u. In this model, the initial positions and momenta of the two electrons are randomly assigned. They satisfy the energy constraint that the total energy equals the negative sum of the first two ionization potentials of the target atom. In Ref. [38], the initial position distributions of the two electrons in phase space are well shown. In our calculations, 4×10^6 trajectories are calculated.

When the initial distribution of the two-electron system is obtained, the evolution of this system in the laser field is determined by the Newtonian equation,

$$\frac{d\mathbf{r}_i(t)}{dt} = \mathbf{p}_i(t),$$

$$\frac{d\mathbf{p}_i(t)}{dt} = -\nabla[V_{ne} + V_{ee} + V_H] - \mathbf{E}(t) - \mathbf{p}_i(t) \times \mathbf{B}(t). \quad (3)$$

Here, $\mathbf{E}(t)$ and $\mathbf{B}(t)$ are the electric and magnetic fields of the laser pulse, respectively. In our calculations, the laser pulse is polarized in the x-y panel and propagates along the z axis. The electric and magnetic field are given by

$$\mathbf{E}(t) = f(t)E_0[\cos(\omega t)\hat{e}_x + \epsilon \sin(\omega t)\hat{e}_y],$$

$$\mathbf{B}(t) = \hat{e}_z \times \mathbf{E}(t)/c, \quad (4)$$

where $f(t) = \exp[-(t/\tau)^2/2]$ is the Gaussian envelope with a full width at half maximum (FWHM) of $2\sqrt{\ln 2}\tau$. E_0 is the amplitude of the electric field, $\omega = 0.057$ a.u. is the central frequency, and ϵ is the laser ellipticity. c is the light speed. We solve the Newtonian equation and record the energy of the two electrons per 0.01 laser cycle. The double ionization event is defined when both electrons have positive energies at the end of the laser pulse.

To test the validity of our model in describing the nondipole effect in strong-field SDI, we first analyze the photon momentum transfer $\langle p_z \rangle$ in SDI of the Ar atom by a circularly polarized laser field. Figure 1(a) shows the mean momentum of the electrons along the laser propagation direction, as a function of the radial momentum. The laser intensity is 2.0 PW/cm². Here, both the first and the second electrons are included because they are indistinguishable in experiment. For such high laser intensity, double ionization dominates by SDI. The dependence of $\langle p_z \rangle$ on the radial momentum $p_\perp$ follows the relation [the dashed line in Fig. 1(a)]

$$\langle p_z \rangle = \frac{p_\perp^2}{2c} + \frac{I_{p1} + I_{p2}}{6c}. \quad (5)$$

According to previous studies [9,14], the second term in Eq. (5) results from the sub-barrier process. In our case, both the first and the second electrons are involved. Therefore, the sub-barrier contribution is the average contribution of the two electrons, i.e., $(I_{p1} + I_{p2})/(6c)$, instead of $I_{p1}/3c$ in the
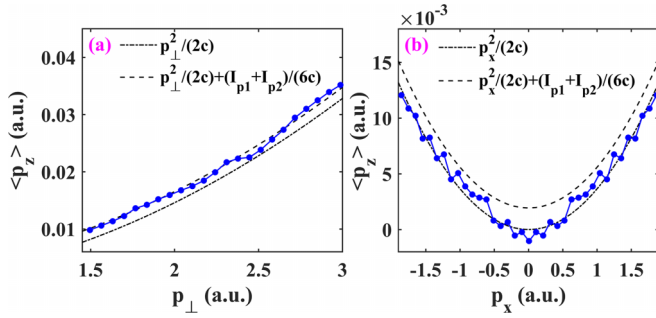
FIG. 1. (a) The mean electron momentum in the light propagation direction $\langle p_z \rangle$ plotted against the radial momentum, $p_\perp = \sqrt{p_x^2 + p_y^2}$. Both electrons in SDI are collected here. The laser is circularly polarized, and the laser intensity is 2.0 PW/cm² and FWHM = 20 fs. The dashed and dotted lines show the predictions given by Eq. (5) and Eq. (6), respectively. (b) Same as (a), but for the linearly polarized laser pulse with laser intensity 1.0 PW/cm².
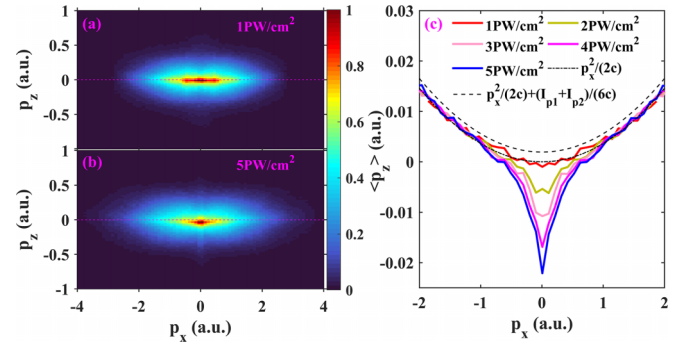

FIG. 2. (a) PEMD in the p_x-p_z plane from SDI by a linearly polarized laser pulse with the intensity of 1.0 PW/cm² and FWHM = 20 fs. (b) Same as (a), but for the laser field with intensity of 5.0 PW/cm². (c) The mean electron momentum in the light propagation direction $\langle p_z \rangle$ plotted against p_x for the laser intensity ranging from 1.0 to 5.0 PW/cm². The dashed and dotted lines show the predictions given by Eq. (5) and Eq. (6), respectively.

case of single ionization. We should note that in previous studies with the semiclassical model [11,32–36], in which the initial distributions of the electrons are given by the Ammosov-Delone-Krainov (ADK) formula, the contribution of the magnetic effect from the sub-barrier process should be added artificially. The result in Fig. 1(a) indicates that the magnetic effect during the sub-barrier process is accurately captured in our model. In previous studies based on the strong-field approximation [14], it has been shown that in tunneling ionization, it is the magnetic field in the sub-barrier process that is responsible for the second term in Eq. (5). In the classical model, electrons are ionized through the over-the-barrier process, where the electrons' energy increases continuously before ionization and becomes ionized when the electron's energy is higher than the potential barrier formed by the combined laser field and Coulomb potential. In this "climbing up" process, the Coulomb force is significant and the interplay between the Coulomb force and the magnetic component of the Lorentz force results in the second term in Eq. (5). It is a surprise that the numerical results from our classical model agree well with the quantum prediction.

Figure 1(b) shows the results in the linearly polarized laser field, where the laser intensity is 1.0 PW/cm². In this case, it has been shown that the momentum shift from the sub-barrier process is approximately canceled by the Coulomb interaction after tunneling [9–11], and thus

$$\langle p_z \rangle \approx \frac{p_x^2}{2c}. \tag{6}$$

The result from our calculations in Fig. 1(b) agrees well with the prediction given by Eq. (6). It indicates that our model is able to accurately describe the magnetic field effect in SDI, both in the ionization process and the Coulomb interaction after ionization. In the following, we focus on revealing the magnetic field effect in SDI induced by linearly polarized laser pulses.

III. RESULTS AND DISCUSSION

Figure 2(a) displays the photoelectron momentum distribution (PEMD) in the (p_x-p_z) panel for SDI by the linearly

polarized laser pulse with the intensity of 1.0 PW/cm². It shows that the asymmetry of the PEMD along the laser propagation direction is not obvious in this case. When the laser intensity is increased to 5.0 PW/cm², as shown in Fig. 2(b), the PEMD for the low-energy electrons reveals significant asymmetry. To quantitatively characterize the intensity dependence of PEMD asymmetry induced by the magnetic field, the mean PEMD in the laser propagation direction $\langle p_z \rangle$ for five different intensities in the range of ∼1.0–5.0 PW/cm² is displayed in Fig. 2(c). For electrons with $|p_x| \gtrsim 1$ a.u., the expectation value $\langle p_z \rangle$ agrees well with the prediction by Eq. (6), and it does not change with laser intensity. However, for the low-energy electrons with $|p_x| \lesssim 1$ a.u., the expectation value deviates from the expected parabolic curve, and the deviation drastically increases with increasing laser intensity. In the case of 5.0PW/cm², $\langle p_z \rangle$ reach up to −0.02 a.u. for $|p_x| \approx 0$.

To reveal the underlying physics of this pronounced momentum shift and its intensity dependence, we focus on the electrons with near-zero final energy ($|p_x| \leqslant 0.1$ a.u.) in the SDI events. Since the low-energy electrons are typically ionized around the peaks of the driving laser waveform, they can quiver around the nucleus and feel strong Coulomb attraction. We categorize the trajectories into two classes based on the closest electron-nucleus distance ($R_{\min} = \text{Min}[\sqrt{x^2 + y^2 + z^2}]$) after ionization, i.e., class I wherein $R_{\min} > 10$ a.u. and class II wherein $R_{\min} < 10$ a.u. In class I, the electron moves away directly after ionization and is referred as the direct electrons, while in class II, the electron suffers a soft rescattering with the parent ion and is referred to as the rescattering electrons. The typical electron trajectories for these two types of electrons are displayed in Figs. 3(a) and 3(b), respectively. The insets display the evolution of the electron-nucleus distance, and the black arrow indicates the time of soft rescattering. For the direct electrons, the displacement induced by the magnetic field (z) is always along the laser propagation direction, while for the rescattering electrons, the electrons abruptly move against the radiation pressure after rescattering, which results in a negative momentum along the z axis. It implies that the rescattering process
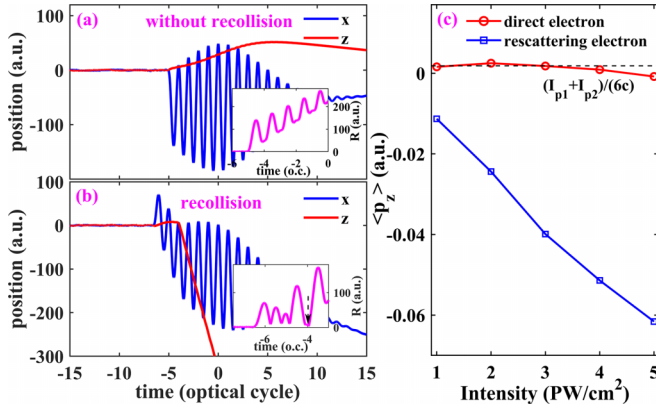
FIG. 3. [(a),(b)] Typical electron trajectories in SDI in the linearly polarized laser field. (a) A trajectory for the electrons without rescattering; (b) a trajectory with soft rescattering. The blue and red lines are the evolution of the coordinates along the laser polarized direction x and laser propagation direction z, respectively. The insets show the distance (R) between the electron and nucleus as a function of time. The black arrow indicates the time of soft rescattering. (c) Expectation value $\langle p_z \rangle$ at the end of the laser pulses as a function of laser intensity. The red and blue lines are the results for the direct electrons and the rescattering electrons, respectively. Note that only the electrons with near-zero ($|p_x| \leqslant 0.1$ a.u.) final energy are analyzed.

is responsible for the negative momentum shift for the low-energy electrons. The respective expectation value $\langle p_z \rangle$ for the direct and rescattering electrons is displayed in Fig. 3(c). The mean value $\langle p_z \rangle$ for the direct electrons agrees well with the under-barrier nondipole shift $(I_{p1} + I_{p2})/6c$, as indicated by the black dashed line. The momentum shift due to the magnetic field after ionization is negligible because $p_x \approx 0$ and thus $p_x^2/2c \approx 0$. However, for the electrons with soft rescattering, the mean momentum $\langle p_z \rangle$ show a significantly negative shift, and this mean momentum decreases rapidly as the laser intensity increases. It indicates that the soft rescattering plays a pivotal role in the pronounced momentum shift against the laser propagation direction shown in Fig. 2(c).

To trace the origination of the pronounced momentum shift and reveal the magnetic field effect in soft rescattering, the evolution of the PEMD in the light-propagation direction (p_z) for the near-zero-energy electrons is displayed in Fig. 4(b). For comparison, the result with the dipole approximation [i.e., the magnetic component Lorentz force in Eq. (3) is switched of] is displayed in Fig. 4(a). Note that the rescattering time t_r of each trajectory is set to zero artificially for better view. Figure 4(a) shows that the p_z distribution diffuses slowly before rescattering, and then quickly splits into two parts due to the recollision process. These two parts represent the two routes of the rescattering electrons, as illustrated in the insets of Figs. 4(c), and 4(e). For route A, the electron returns to the parent ion from the positive laser propagation direction and experiences negative Coulomb force, which results in negative p_z, as displayed in Figs. 4(c) and 4(d). The circumstance for route B, shown in Figs. 4(e) and 4(f), is the opposite of route A, which results in a positive p_z. Without the magnetic field
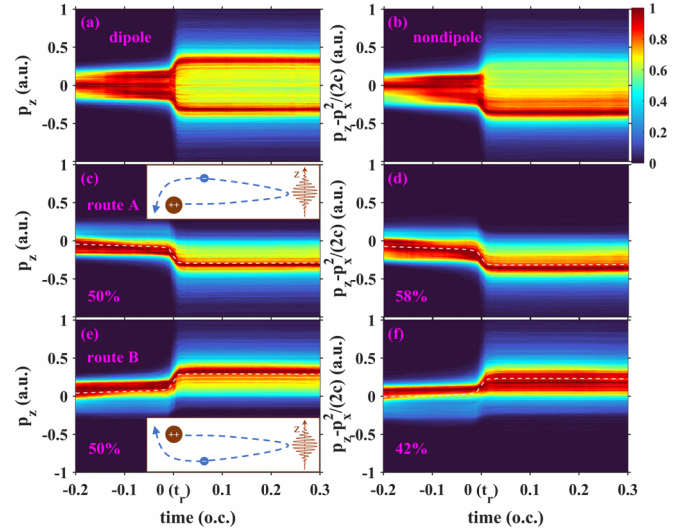

FIG. 4. [(a),(b)] The evolution of the PEMD along the laser propagation direction for the rescattering electrons for the laser intensity 5 PW/cm^2. [(c),(d)] and [(e),(f)] are the same as [(a),(b)], but for route A [(c),(d)], where the electron returns from the positive direction of the laser propagation direction [as illustrated by the inset in (c)], and route B [(e),(f)], where the electron returns from the negative direction of the laser propagation direction [as illustrated by the inset in (e)]. The white-dashed line in [(c)–(f)] shows the mean value of the corresponding distribution evolution. The left [(a),(c),(e)] and right [(b),(d),(f)] panels display the results obtained by HPCM with the dipole approximation and considering the magnetic field effect, respectively. Note that only 0.5 optical cycle evolution in the vicinity of the recollision time (t_r) is shown, and the recollision time of each trajectory is set to zero. The distribution is normalized individually with respect to the maximum at each time.

effect, as shown in Figs. 4(a), 4(c), and 4(e), the probabilities of these two routes are the same and both have the equal probability of 50%. Therefore, the p_z distribution within the dipole approximation is symmetric about $p_z = 0$, and then $\langle p_z \rangle = 0$, while the ratio of these two routes is significantly changed when the magnetic field is included, as shown in Figs. 4(b), 4(d), and 4(f). For the intensity of 5.0 PW/cm^2, the probability of route A increases to 58% and it decreases to 42% for route B, manifesting as an asymmetric p_z distribution, shown in Fig. 4(b), which results in a pronounced negative $\langle p_z \rangle$, shown in Fig. 2(c).

This asymmetric probabilities of these two routes can be understood by surveying the displacement of the electrons induced by the magnetic field. During the ionization and rescattering, due to the magnetic component of the Lorentz force, the electron has a tiny displacement along the laser propagation direction. It means that the electron with small negative initial momentum p_z (which belongs to route B within the dipole approximation) moves to the positive z axis before the soft rescattering. These electrons return back to the parent ion with positive displacement in the z direction, and receive negative momentum p_z during the soft rescattering with the parent ion, forming route A. As a result, the probability increases for route A and decreases for route B when the magnetic field effect is included. To show this picture more clearly, the time evolution of the mean position of the
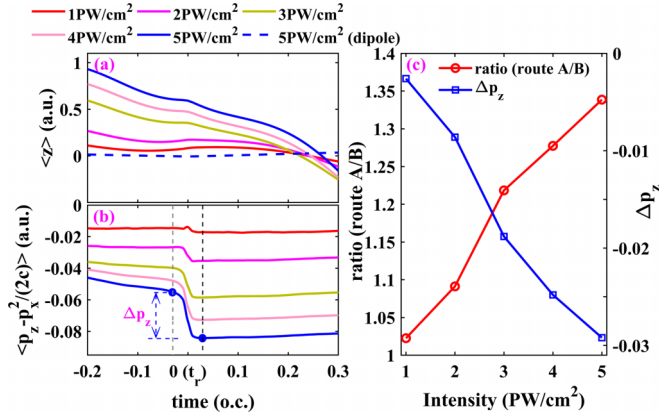
FIG. 5. (a) Evolution of the electrons' mean displacement along the z axis for different laser intensities. The blue dashed line represents the results obtained by the HPCM with the dipole approximation. (b) Evolution of the mean deviation of the electron momentum from the classical prediction along the laser propagation direction, i.e., $\langle p_z - p_x^2/(2c) \rangle$. (c) The laser intensity dependence of the ratio between route A and route B (red circles, left axis). The laser intensity dependence of the momentum jump (the right axis) due to the soft rescattering, which is obtained by calculating the momentum difference after $(t_r + 0.03T)$ and before $(t_r - 0.03T)$ the rescattering [as indicated by the dashed black line and the dashed gray line in (b), respectively].

FIG. 6. (a) The traveling time dependence of the mean electron's position along the z axis just before the recollision, $0.03T$. (b) The traveling time dependence of the ratio between route A and route B. (c) The traveling time dependence of mean momentum distribution along the laser propagation direction at the end of the laser pulses. The results, by performing the HPCM with the dipole approximation, are also shown by the blue line in [(a)–(c)] for comparison. (d) Mean electron momentum $\langle p_z \rangle$ in the light-propagation direction as a function of p_x for the FWHM of 6, 10, 15, 20 fs. The laser intensity is 5 PW/cm^2.

electrons in the laser-propagation direction is displayed in Fig. 5(a). In the dipole approximation, the mean position $\langle z \rangle$ is always zero (dashed blue line), indicating that the spatial distribution of the electrons along the z axis is symmetric before and after the recollision. However, when the magnetic field effect is included, the mean position $\langle z \rangle$ is significantly shifted to the z positive direction before the recollision. This displacement of the electrons induced by the magnetic field effect results in the asymmetric probabilities of routes A and B. The displacement increases with the laser intensities due to the larger Lorentz force, which causes more asymmetric probabilities of these two rescattering routes, as displayed by the red line in Fig. 5(c).

The ratio of routes A and B determines the deviation of the mean p_z distribution from the prediction of Eq. (6) [the parabolic curve in Fig. 2(c)]. In Fig. 5(b), the time evolution of this mean deviation, $\langle p_z - p_x^2/(2c) \rangle$, is displayed. A significant momentum jump Δp_z appears due to the electron-ion rescattering. The Δp_z is obtained by calculating the momentum difference 0.03 T after and before the rescattering [as indicated by the dashed black line and the dashed gray line in Fig. 5(b), respectively]. This jump increases with laser intensity. Figure 5(c) quantitatively shows the laser intensity dependence of this momentum jump Δp_z (the blue curve). It indicates a larger momentum shift to the negative direction during the soft rescattering for the higher laser intensities.

So far, we have shown that the counterintuitive mean p_z distribution is due to the magnetic field induced displacement along the laser-propagation direction, which increases with laser intensity. This displacement results in an asymmetric spatial distribution of the electron before the rescattering. This asymmetry results in the negative momentum along the laser-
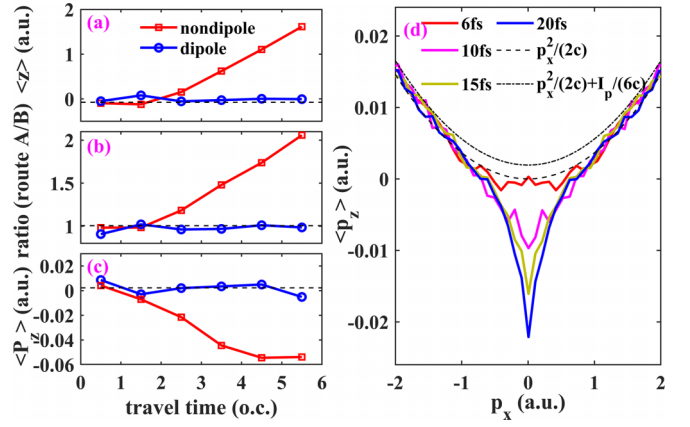
propagation direction during the soft rescattering. The degree of the asymmetry and the value of the negative momentum depend on the longitudinal displacement before rescattering. The large displacement results in the large negative momentum.

This displacement is induced by the magnetic field. It not only depends on the laser intensity, but also increases with the traveling time between ionization and the soft rescattering. The longer traveling time induces larger displacement along the laser-propagation direction. Driven by the strong laser field, the soft rescattering could occur at the first or the later returns. Figure 6(a) shows mean displacement $\langle z \rangle$ as a function of the traveling time. It confirms that the displacement due to the magnetic field increases with the traveling time. Correspondingly, the ratio between routes A and B increases with the traveling time [Fig. 6(b)]. As a result, the negative shift in $\langle p_z \rangle$ increases with the traveling time, as shown in Fig. 6(c).

As the pulse duration increases, the contribution at later returns increases. Thus, it can be expected that the negative shift in $\langle p_z \rangle$ increases with the duration of the laser pulse. Figure 6(d) shows the momentum $\langle p_z \rangle$ as a function of p_x at different pulse durations. It is clearly shown that the dip is more obvious for the longer pulse durations.

IV. CONCLUSIONS

In summary, we have investigated the magnetic field effect in SDI of Ar with the ND-HPCM, which fully accounts for the magnetic field in time propagation. We have shown that this model can accurately describe the magnetic effect in strong-field ionization. We find that the magnetic field induces a displacement of the electrons along the laser-propagation direction, which results in an asymmetric spatial

distribution of the photoelectron before the soft rescattering, i.e., more electrons rescattering with the parent ion with positive impact parameter along the laser-propagation direction. As a consequence, the mean momentum distribution along the laser-propagation direction shows a pronounced linear momentum transfer against the radiation pressure for the low-energy photoelectron. The displacement induced by the magnetic field depends on the laser intensity and the traveling time of the photoelectrons. Thus, the linear momentum transfer can be controlled by the laser intensity and pulse duration. A larger negative momentum transfer for low-energy electrons is obtained in a more intense laser field with longer pulse duration, which is a benefit to observe this effect in experiment. Our work deepens the understanding of the magnetic field role in strong-field ionization and provides an intuitive insight into the magnetic field effect in the laser-induced recollision.

[1] H. R. Reiss, Limits on tunneling theories of strong-field ionization, Phys. Rev. Lett. **101**, 043002 (2008).

[2] H. R. Reiss, The tunnelling model of laser-induced ionization and its failure at low frequencies, J. Phys. B **47**, 204006 (2014).

[3] D. P. Crawford and H. R. Reiss, Relativistic ionization of hydrogen by linearly polarized light, Opt. Express **2**, 289 (1998).

[4] C. T. L. Smeenk, L. Arissian, B. Zhou, A. Mysyrowicz, D. M. Villeneuve, A. Staudte, and P. B. Corkum, Partitioning of the linear photon momentum in multiphoton ionization, Phys. Rev. Lett. **106**, 193002 (2011).

[5] A. Ludwig, J. Maurer, B. W. Mayer, C. R. Phillips, L. Gallmann, and U. Keller, Breakdown of the dipole approximation in strong-field ionization, Phys. Rev. Lett. **113**, 243001 (2014).

[6] N. Haram, I. Ivanov, H. Xu, K. T. Kim, A. Atia-tul-Noor, U. S. Sainadh, R. D. Glover, D. Chetty, I. V. Litvinyuk, and R. T. Sang, Relativistic nondipole effects in strong-field atomic ionization at moderate intensities, Phys. Rev. Lett. **123**, 093201 (2019).

[7] A. Hartung, S. Brennecke, K. Lin, D. Trabert, K. Fehre, J. Rist, M. S. Schöffler, T. Jahnke, L. Ph. H. Schmidt, M. Kunitski, M. Lein, R. Dörner, and S. Eckart, Electric nondipole effect in strong-field ionization, Phys. Rev. Lett. **126**, 053202 (2021).

[8] B. Willenberg, J. Maurer, B. W. Mayer, and U. Keller, Subcycle time resolution of multi-photon momentum transfer in strong-field ionization, Nat. Commun. **10**, 5548 (2019).

[9] A. Hartung, S. Eckart, S. Brennecke, J. Rist, D. Trabert, K. Fehre, M. Richter, H. Sann, S. Zeller, K. Henrichs, G. Kastirke, J. Hoehl, A. Kalinin, M. S. Schöffler, T. Jahnke, L. Ph. H. Schmidt, M. Lein, M. Kunitski, and R. Dörner, Magnetic fields alter strong-field ionization, Nat. Phys. **15**, 1222 (2019).

[10] K. Lin, X. Chen, S. Eckart, H. Jiang, A. Hartung, D. Trabert, K. Fehre, J. Rist, L. Ph. H. Schmidt, M. S. Schöffler, T. Jahnke, M. Kunitski, F. He, and R. Dörner, Magnetic-field effect as a tool to investigate electron correlation in strong-field ionization, Phys. Rev. Lett. **128**, 113201 (2022).

[11] K. Lin, S. Brennecke, H. Ni, X. Chen, A. Hartung, D. Trabert, K. Fehre, J. Rist, X.-M. Tong, J. Burgdörfer, L. Ph. H. Schmidt, M. S. Schöffler, T. Jahnke, M. Kunitski, F. He, M. Lein, S. Eckart, and R. Dörner, Magnetic-field effect in high-order above-threshold ionization, Phys. Rev. Lett. **128**, 023201 (2022).

[12] N. Haram, H. Xu, I. Ivanov, D. Chetty, I. Litvinyuk, and R. T. Sang, Strong-field ionization of argon: Electron momentum spectra and nondipole effects, Phys. Rev. A **105**, 023522 (2022).

[13] A. S. Titi and G. W. F. Drake, Quantum theory of longitudinal momentum transfer in above-threshold ionization, Phys. Rev. A **85**, 041404(R) (2012).

[14] M. Klaiber, E. Yakaboylu, H. Bauke, K. Z. Hatsagortsyan, and C. H. Keitel, Under-the-barrier dynamics in laser-induced relativistic tunneling, Phys. Rev. Lett. **110**, 153004 (2013).

[15] S. Chelkowski, A. D. Bandrauk, and P. B. Corkum, Photon momentum sharing between an electron and an ion in photoionization: From one-photon (photoelectric effect) to multiphoton absorption, Phys. Rev. Lett. **113**, 263005 (2014).

[16] P.-L. He, D. Lao, and F. He, Strong field theories beyond dipole approximations in nonrelativistic regimes, Phys. Rev. Lett. **118**, 163203 (2017).

[17] H. Ni, S. Brennecke, X. Gao, P.-L. He, S. Donsa, I. Březinová, F. He, J. Wu, M. Lein, X.-M. Tong, and J. Burgdörfer, Theory of subcycle linear momentum transfer in strong-field tunneling ionization, Phys. Rev. Lett. **125**, 073202 (2020).

[18] J. Liang, Y. Zhou, W.-C. Jiang, M. Yu, M. Li, and P. Lu, Zeeman effect in strong-field ionization, Phys. Rev. A **105**, 043112 (2022).

[19] H. R. Reiss, Relativistic strong-field photoionization, J. Opt. Soc. Am. B **7**, 574 (1990).

[20] S. Brennecke and M. Lein, Nondipole modification of the ac Stark effect in above-threshold ionization, Phys. Rev. A **104**, L021104 (2021).

[21] M. M. Lund and L. B. Madsen, Nondipole photoelectron momentum shifts in strong-field ionization with mid-infrared laser pulses of long duration, J. Phys. B: At. Mol. Opt. Phys. **54**, 165602 (2021).

[22] K. Lin, S. Eckart, A. Hartung, D. Trabert, K. Fehre, J. Rist, L. Ph. H. Schmidt, M. S. Schöffler, T. Jahnke, M. Kunitski, and R. Dörner, Photoelectron energy peaks shift against the radiation pressure in strong-field ionization, Sci. Adv. **8**, eabn7386 (2022).

[23] J. Tan, S. Xu, X. Han, Y. Zhou, M. Li, W. Cao, Q. Zhang, and P. Lu, Resolving and weighing the quantum orbits in strong-field tunneling ionization, Adv. Photon. **3**, 035001 (2021).

[24] J. Liang, Y. Zhou, Y. Liao, W.-C. Jiang, M. Li, and P. Lu, Direct visualization of deforming atomic wavefunction in

ultraintense high-frequency laser pulses, Ultrafast Sci. **2022**, 9842716 (2022).

[25] J. Liu, Q. Z. Xia, J. F. Tao, and L. B. Fu, Coulomb effects in photon-momentum partitioning during atomic ionization by intense linearly polarized light, Phys. Rev. A **87**, 041403(R) (2013).

[26] J. Maurer, B. Willenberg, J. Daněk, B. W. Mayer, C. R. Phillips, L. Gallmann, M. Klaiber, K. Z. Hatsagortsyan, C. H. Keitel, and U. Keller, Probing the ionization wave packet and recollision dynamics with an elliptically polarized strong laser field in the nondipole regime, Phys. Rev. A **97**, 013404 (2018).

[27] J. Daněk, M. Klaiber, K. Z. Hatsagortsyan, C. H. Keitel, B. Willenberg, J. Maurer, B. W. Mayer, C. R. Phillips, L. Gallmann, and U. Keller, Interplay between Coulomb-focusing and non-dipole effects in strong-field ionization with elliptical polarization, J. Phys. B **51**, 114001 (2018).

[28] S. Chelkowski, A. D. Bandrauk, and P. B. Corkum, Photon-momentum transfer in multiphoton ionization and in time-resolved holography with photoelectrons, Phys. Rev. A **92**, 051401(R) (2015).

[29] S. Brennecke and M. Lein, Strong-field photoelectron holography beyond the electric dipole approximation: A semiclassical analysis, Phys. Rev. A **100**, 023413 (2019).

[30] B. Willenberg, J. Maurer, U. Keller, J. Daněk, M. Klaiber, N. Teeny, K. Z. Hatsagortsyan, and C. H. Keitel, Holographic interferences in strong-field ionization beyond the dipole approximation: The influence of the peak and focal-volume-averaged laser intensities, Phys. Rev. A **100**, 033417 (2019).

[31] S. Brennecke and M. Lein, High-order above-threshold ionization beyond the electric dipole approximation, J. Phys. B **51**, 094005 (2018).

[32] F. Sun, X. Chen, W. Zhang, J. Qiang, H. Li, P. Lu, X. Gong, Q. Ji, K. Lin, H. Li, J. Tong, F. Chen, C. Ruiz, J. Wu, and F. He, Longitudinal photon-momentum transfer in strong-field double ionization of argon atoms, Phys. Rev. A **101**, 021402(R) (2020).

[33] A. Emmanouilidou and T. Meltzer, Recollision as a probe of magnetic-field effects in nonsequential double ionization, Phys. Rev. A **95**, 033405 (2017).

[34] A. Emmanouilidou, T. Meltzer, and P. B. Corkum, Non-dipole recollision-gated double ionization and observable effects, J. Phys. B **50**, 225602 (2017).

[35] G. P. Katsoulis, M. B. Peters, A. Staudte, R. Bhardwaj, and A. Emmanouilidou, Signatures of magnetic-field effects in nonsequential double ionization manifesting as backscattering for molecules versus forward scattering for atoms, Phys. Rev. A **103**, 033115 (2021).

[36] X. Chen, C. Ruiz, F. He, and J. Zhang, Mapping initial transverse momenta of tunnel-ionized electrons to rescattering double ionization in nondipole regimes, Opt. Express **28**, 14884 (2020).

[37] J. S. Cohen, Quasiclassical effective Hamiltonian structure of atoms with $z = 1$ to 38, Phys. Rev. A **51**, 266 (1995).

[38] Y. Zhou, C. Huang, Q. Liao, and P. Lu, Classical simulations including electron correlations for sequential double ionization, Phys. Rev. Lett. **109**, 053004 (2012).

[39] S. Liu, D. Ye, and J. Liu, Classical simulation of spin-tagged collisional ionization at near-threshold energies, J. Phys. B **53**, 145005 (2020).

[40] Y. Zhou, M. Li, Y. Li, A. Tong, Q. Li, and P. Lu, Dissection of electron correlation in strong-field sequential double ionization using a classical model, Opt. Express **25**, 8450 (2017).

[41] G. Pandey, S. Ghosh, and A. K. Tiwari, Dissociative ionization of the H_2 molecule under a strong elliptically polarized laser field: Carrier-envelope phase and orientation effect, Phys. Chem. Chem. Phys. **24**, 24582 (2022).

[42] Y. Zhou, Q. Zhang, C. Huang, and P. Lu, Classical description of strong-field double ionization by elliptical laser pulses, Phys. Rev. A **86**, 043427 (2012).

[43] H. Jiang and F. He, Semiclassical study of nonsequential triple ionization of Ar in strong laser fields, Phys. Rev. A **104**, 023113 (2021).